A Diencephalic Dopamine Source Provides Input to the Superior Colliculus, where D1 and D2 Receptors Segregate to Distinct Functional Zones

Citation: Bolton, Andrew D., Yasunobu Murata, Rory Kirchner, Sung-Yon Kim, Andrew Young, Tru Dang, Yuchio Yanagawa, and Martha Constantine-Paton. "A Diencephalic Dopamine Source Provides Input to the Superior Colliculus, Where D1 and D2 Receptors Segregate to Distinct Functional Zones." Cell Reports 13, no. 5 (November 2015): 1003–15.

As Published: http://dx.doi.org/10.1016/j.celrep.2015.09.046

Publisher: Elsevier

Persistent URL: http://hdl.handle.net/1721.1/101615

Version: Final published version: final published article, as it appeared in a journal, conference proceedings, or other formally published context

Article

Cell Reports

A Diencephalic Dopamine Source Provides Input to the Superior Colliculus, where D1 and D2 Receptors Segregate to Distinct Functional Zones

Graphical Abstract

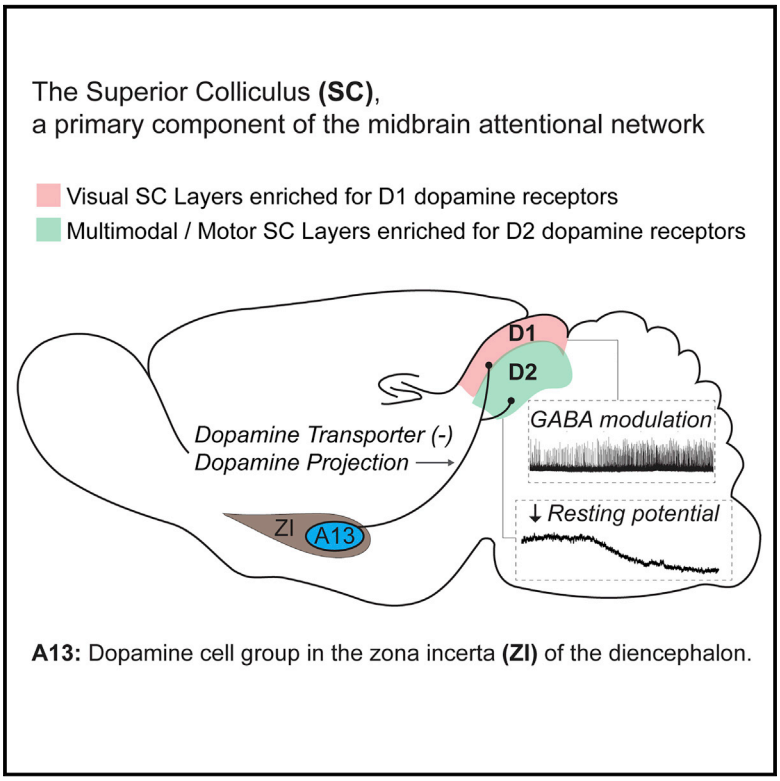

A13: Dopamine cell group in the zona incerta **(ZI)** of the diencephalon.

Authors

Andrew D. Bolton, Yasunobu Murata, Rory Kirchner, ..., Tru Dang, Yuchio Yanagawa, Martha Constantine-Paton

Correspondence

andrew.d.bolton@gmail.com

In Brief

Bolton et al. have provided a detailed anatomical, genetic, and electrophysiological characterization of the dopamine system in the midbrain superior colliculus. These findings lay the groundwork for understanding how dopamine may influence the colliculus's ability to allocate attention and orienting movements to specific regions of space.

Highlights

- RNA-seq describes dopamine-related gene expression in the superior colliculus (SC)
- $D1^+$ and $D2^+$ neurons segregate to functionally distinct SC layers
- $D1^+$ and $D2^+$ neurons in the SC differentially express the inhibitory marker VGAT
- Retrograde tracing points to A13 as the source of dopamine to the SC
- Patch-clamp analysis suggests functional consequences of SC dopamine

Accession Numbers

GSM1872016
GSM1872017
GSM1872018

Bolton et al., 2015, Cell Reports *13*, 1003–1015
November 3, 2015 ©2015 The Authors
http://dx.doi.org/10.1016/j.celrep.2015.09.046

Cell Reports
Article

A Diencephalic Dopamine Source Provides Input to the Superior Colliculus, where D1 and D2 Receptors Segregate to Distinct Functional Zones

Andrew D. Bolton,[1,4,*] Yasunobu Murata,[1] Rory Kirchner,[1] Sung-Yon Kim,[2] Andrew Young,[1] Tru Dang,[1] Yuchio Yanagawa,[3] and Martha Constantine-Paton[1]
[1]McGovern Institute for Brain Research, Massachusetts Institute of Technology, Cambridge, MA 02139, USA
[2]Picower Institute for Learning and Memory, Massachusetts Institute of Technology, Cambridge, MA 02139, USA
[3]Department of Genetic and Behavioral Neuroscience, Gunma University Graduate School of Medicine, 3-39-22 Showa-machi, Maebashi 371-8511, Japan
[4]Present address: Engert Lab, Harvard University Biolabs, 16 Divinity Avenue, Cambridge, MA 02139, USA
*Correspondence: andrew.d.bolton@gmail.com
http://dx.doi.org/10.1016/j.celrep.2015.09.046

SUMMARY

Modulation of neural responses is frequently observed in the superior colliculus (SC), a retinorecipient midbrain structure that controls orienting and the localization of attention. Although behavioral contingencies that influence SC responses are well documented, the neural pathways and molecular mechanisms responsible for this modulation are not completely understood. Here, we illustrate a dopaminergic system that strongly impacts neural responses in the SC. After using RNA sequencing (RNA-seq) to detail the transcriptome of dopamine-related genes in the SC, we show that D1 receptors are enriched in the superficial visual SC, while D2 receptors segregate to the intermediate multimodal/motor SC. Retrograde injections into the SC consistently label A13, a small dopamine cell group located in the zona incerta. We surmise that A13 mimics dopaminergic effects that we observed in SC slices, which suggests that dopamine in the SC may reduce the tendency of an animal to orient or attend to salient stimuli.

INTRODUCTION

Neurons in the superior colliculus (SC) exhibit different responses to the same stimulus based on current behavioral demands (Knudsen, 2011; Basso and Wurtz, 1998; Wurtz and Mohler, 1976; Ikeda and Hikosaka, 2003, 2007). Understanding the neural basis of this modulation is critical, because the SC exerts an incredible amount of control over spatial attention and behavioral target selection, with the ability to override current behavioral tasks to shift attention to new, more salient environmental stimuli (Merker, 1980; Müller et al., 2005; Lovejoy and Krauzlis, 2010; Krauzlis et al., 2004). Two pathways that modulate the SC have already been functionally described, including the cholinergic and GABAergic nucleus isthmi (Goddard et al., 2014; Gruberg et al., 2006; Dudkin and Gruberg, 2003) and the GABAergic substantia nigra pars reticulata (Hikosaka and Wurtz, 1985; Basso and Wurtz, 2002; Knudsen, 2011). However, although the neuromodulator dopamine has been shown to alter sensory responses to visual input in frontal cortex (Jacob et al., 2013), odor stimuli in the olfactory forebrain (Schärer et al., 2012), and auditory stimuli in A1 (Happel et al., 2014), a detailed anatomical and electrophysiological description of its impact on the SC has never been shown. We therefore used genetic, anatomical, and electrophysiological approaches in order to understand dopamine's influence on SC function.

Modulation of the SC must be understood in the context of the complex SC structure, which contains multiple interconnected neural layers that are ostensibly distinct in terms of electrophysiology (Isa and Hall, 2009), functionality (Northmore et al., 1988; Dean et al., 1989), and molecular expression (Illing, 1996; Mize et al., 1992; Behan et al., 2002). The superficial SC consists of three layers (the stratum zonalae [SZ], stratum griesium superficialae [SGS], and stratum opticum [SO]) that receive direct input from the retina and contain neurons with exclusively visual receptive fields (Huerta and Harting, 1984b; Dräger and Hubel, 1975). Single neurons in the largest superficial layer, the SGS, receive converging input from both V1 and retinal ganglion cell axons that terminate along the SC surface in a topographic "visual map" of contralateral space (Sperry, 1963; Phillips et al., 2011; Huerta and Harting, 1984b); these retinal axons enter the SC via the SO ventral to the SGS and give rise to activity in superficial SC neurons that encodes the spatial locations of salient visual stimuli.

The visual SC layers project ventrally to the intermediate SC, which translates the topographic map of visual space to intermediate layer neurons (Helms et al., 2004). However, unlike the purely visual superficial SC, the intermediate SC layers (the stratum griesium intermediale [SGI] and stratum album intermediale [SAI]) are multimodal, responding topographically to somatosensory and auditory input in addition to vision (Huerta and Harting, 1984a; Dräger and Hubel, 1975). The intermediate SC also contains a "motor map"; that is, activation of neurons in these layers

evokes orienting movements (Robinson, 1972; Schiller and Stryker, 1972; Northmore et al., 1988; Dean et al., 1986; Ewert, 1984), or shifts in covert attention (Müller et al., 2005), to prescribed locations in space. The alignment of SC sensory and motor maps means that salient sensory input can induce spatially precise movements or focal attention toward interesting stimuli (Ingle, 1975).

Here, we describe a dopaminergic modulatory pathway that terminates in the SC, where D1 and D2 receptors are arranged in a behaviorally relevant pattern: D1 receptors are enriched in the superficial visual SC, while D2 receptors are concentrated in the multimodal/motor SC layers. Dopamine, which is found at higher levels in the SC than the frontal cortex or hippocampus (Versteeg et al., 1976), arises from a small diencephalic cell group called A13 and possibly from the locus coeruleus, the only two TH^+ brain regions shown here to consistently receive retrograde labeling from SC injections. We use transcriptome profiling as well as anatomical and patch-clamp methods to describe the specifics of dopamine uptake, metabolism, and electrophysiological function within the SC. Overall, our results lay the groundwork for understanding how dopamine may modulate SC-mediated attention shifts and orienting behaviors.

RESULTS

Characterizing the Dopamine Transcriptome in the SC

An ongoing study in our laboratory has characterized the transcriptome within the superficial and intermediate SC layers of the 3-week-old rat (R.K. and M.C.P., unpublished data). Three samples of RNA were sequenced, each containing three or four superior colliculi (Figure 1A). Figure 1B shows the expression of all transcripts related to the dopamine system in the SC, arranged into receptor-related genes and uptake/breakdown-related genes. We observed strong expression of only two dopamine receptor subtypes in the SC: *Drd1a*, which codes for the D1 dopamine receptor, and *Drd2*, which codes for the D2 dopamine receptor (1.88 ± 0.27 FPKM [fragments per kilobase per million reads] and 5.53 ± 0.15 FPKM, respectively; Figure 1B [see the Figure 1 legend for an explanation of FPKM]; Trapnell et al., 2010). By comparison, genes coding the two most common NMDA receptor subtypes in the brain, *Grin2B* and *Grin2A*, show average FPKM values similar to *Drd1a* and *Drd2*, respectively (2.96 and 7.07 FPKM). *Darpp32* (aka *Pppr1r1b*), a phosphatase inhibitor known to facilitate dopamine receptor signaling (Hemmings et al., 1984), is expressed on the order of *Drd2* (4.39 ± 0.94 FPKM), indicating a prominent role in the SC.

With respect to the breakdown and clearance of synaptic dopamine, genes encoding the breakdown enzymes COMT (catechol-O-methyltransferase) and MAO (monoamine oxidase) are strongly expressed in the SC (*Comt* 18.66 ± 3.50 FPKM, *Maoa* 20.49 ± 1.50 FPKM, *Maob* 14.93 ± 1.35 FPKM). Breakdown, however, can only occur after dopamine is transported into neurons or glia, because soluble COMT, MAOA, and MAOB proteins are all cytosolic and membrane-bound COMT is oriented intracellularly (Schott et al., 2010). The dopamine and norepinephrine transporters (DAT and NET) are candidate uptake mechanisms, but we did not observe expression of *Dat* or *Net* in the SC (Figure 1B). Our studies also suggest that DAT is not even pre-synaptically expressed in SC dopamine terminals (see Results), leading us to search our RNA sequencing (RNA-seq) data for an alternative method of dopamine clearance in the SC.

mRNA for a recently described high-capacity dopamine transporter, *Pmat* (plasma membrane monoamine transporter; Duan and Wang, 2010), is the only candidate transporter that is highly expressed in the SC (9.43 ± 2.98 FPKM; Figure 1B). This elevated expression level is confirmed by a recent immunohistochemistry study showing that the superficial and intermediate SC layers are two of the most highly enriched regions of the brain for PMAT protein (Dahlin et al., 2007). Another class of recently described organic cation transporters does not appear at high levels in the SC (*Emt* 0.26 ± 0.06 FPKM, *Oct1* 0.56 ± 0.20 FPKM, *Oct2* 0.02 ± 0.02 FPKM; Haag et al., 2004; Busch et al., 1996; Gründemann et al., 1998).

Mthfr (methyl tetrahydrofolate reductase) is significantly expressed in the SC (3.26 ± 0.42 FPKM). The MTHFR enzyme is required for dopamine breakdown, as it supplies COMT with methyl groups for dopamine methylation (Tunbridge et al., 2008). Our sequencing results therefore suggest that the main mode of action following dopamine release in the SC is activation of D1 and D2 dopamine receptors, uptake after receptor activation into post-synaptic cells via PMAT, and eventual breakdown via COMT/MAO/MTHFR-mediated metabolism.

$D1^+$ and $D2^+$ Cells Are Segregated in the SC

We next characterized the collicular locations of the two highly expressed dopamine receptors from our RNA-seq data as a first step toward understanding dopamine's effect on SC function. $D1^+$ and $D2^+$ neurons were visualized using mice expressing tdTomato under the *Drd1a* promoter (D1-tdTom; Ade et al., 2011) and enhanced GFP under the *Drd2* promoter (D2-EGFP; Gong et al., 2003). We immediately noticed a remarkable laminar pattern of dopamine receptor expression. $D1^+$ neurons were enriched in the superficial visual layers of the SC, while D2 expression was scarce in this area (Figures 1C–1E). D2-expressing neurons were instead enriched ventral to the SGS, with strongest expression in the intermediate SC (Figures 1C–1E). In total, 29,343 SC neurons (identified by NeuN immunostaining) were counted in our D1-tdTom × D2-EGFP samples: similar proportions of SC neurons expressed D1 and D2 receptors (11.3% $D1^+$, 9.4% $D2^+$). Only 1.2% of SC neurons were both $D1^+$ and $D2^+$; double-labeled neurons did not appear to show any specific spatial arrangement within the SC (Figure 1C). Overall, $D2^+$ neurons were located significantly deeper in the SC than $D1^+$ cells ($p < 0.0001$; Figures 1D and 1E; 262.23 μm versus 462.02 μm median depth from dorsal SC surface). See Table 1 for counts in the rostral, medial, and caudal planes of all D1 and D2 cells.

Characterizing the Inhibitory/Excitatory Identity of D1 and D2 Neuron Populations

Identifying $D1^+$ and $D2^+$ neurons as excitatory or inhibitory is necessary for understanding how these cells operate within the SC circuit. D1-tdTom and D2-tdTom (D2-Cre × floxed-tdTomato) mice were therefore crossed to a line expressing

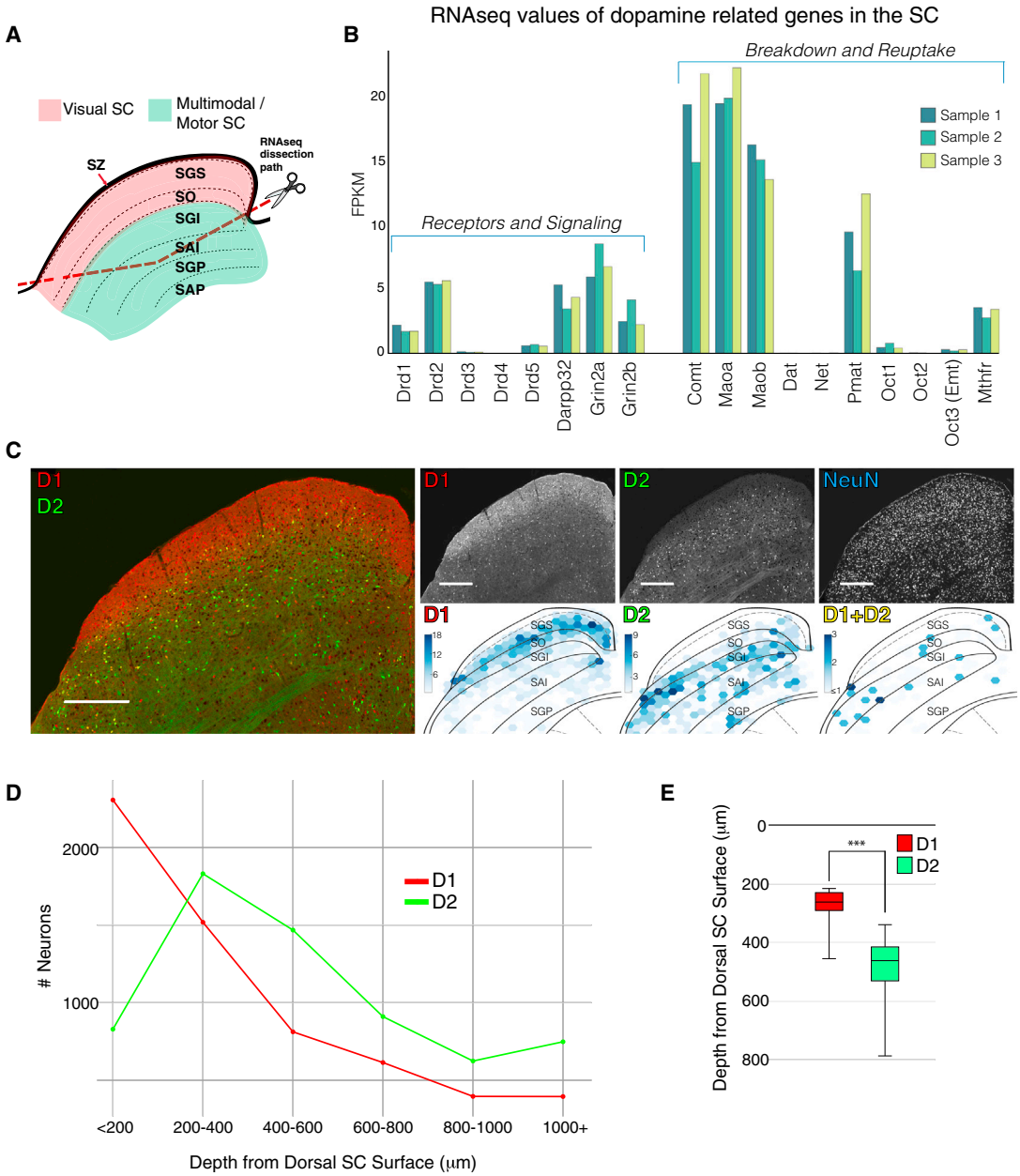

Figure 1. RNA Sequencing Shows Significant Expression of D1 and D2 Dopamine Receptors, which Are Segregated within the SC

(A) Crowns of the superior colliculus were dissected from P20 rats. Tissue samples contained the superficial SC, intermediate gray (SGI), and part of the intermediate white (SAI) layers.

(B) RNA-seq values for dopamine-related genes in the SC are reported in fragments per kilobase per million reads (FPKM). FPKM normalizes the amount of reads observed to the length of the gene, preventing large genes from being over-represented in the analysis and small genes from being under-represented.

(C) D1-tdTom mice were crossed to D2-EGFP mice to produce a D1-tdTom × D2-EGFP double-transgenic mouse. Two-dimensional (2D) histograms indicate $D1^+$ or $D2^+$ cell density for each 80-μm-wide hexagon of collicular space. D1-tdTom expression is enriched in the superficial SC, while D2-EGFP is more highly expressed in the intermediate SC. Total numbers of cells counted across three animals are correlated to bin color in legends left of each panel. Unlike $D1^+$ and $D2^+$ neurons individually, $D1^+$ $D2^+$ neurons showed no particular spatial pattern. Scale bars represent 300 μm.

(D) Scatterplot showing the distribution of $D1^+$ and $D2^+$ neurons binned by depth from the dorsal SC surface. All neurons counted from all coronal planes of three D1-tdTom × D2-EGFP, three D1-tdTom × VGAT-Venus, and three D2-tdTom × VGAT-Venus animals were pooled.

(E) Boxplot showing the distribution of median depths of D1 and D2 neurons from the dorsal SC surface. Median depths were calculated in each slice (rostral, middle, and caudal) of three D1-tdTom × D2-EGFP, three D1-tdTom × VGAT-Venus, and three D2-tdTom × VGAT-Venus samples, totaling 18 medians per distribution. $D2^+$ neurons were significantly deeper in the SC than $D1^+$ cells (***$p < 0.0001$, D1: 262.23 μm versus D2: 462.02 μm median depth). Ends of whiskers are maximum and minimum of the distributions, box edges are first and third quartiles, and lines inside boxes are medians.

Table 1. Total Neuron Counts of D1, D2, and Dopamine Receptor Overlap with VGAT

	D1-tdTom × D2-EGFP				D1-tdTom × VGAT-Venus		D2-tdTom × VGAT-Venus	
	$D1^+$	$D2^+$	$D1^+$ $D2^+$	NeuN	$D1^+$ $VGAT^+$	$D1^+$ $VGAT^-$	$D2^+$ $VGAT^+$	$D2^+$ $VGAT^-$
Rostral	763	878	91	10,787	520	510	503	960
Middle	1,166	787	118	11,018	726	443	608	952
Caudal	1,036	737	140	7,538	547	330	381	604
Total	2,965	2,402	349	29,343	1,793	1,293	1,492	2,516

VGAT, vesicular GABA transporter; D1, dopamine receptor 1; D2, dopamine receptor 2; NeuN, neuronal nuclei stain.

the yellow fluorescent protein Venus in neurons expressing the vesicular GABA transporter (VGAT), which is only found in GABAergic SC neurons (Wang et al., 2009).

Overall, $D1^+$ SC neurons expressed VGAT at a 58% rate (1,793/3,076), Figure 2A; Table 1). Critically, however, seven out of every ten $D1^+$ cells were $VGAT^+$ in the superficial SC (<200 μm deep, 69.4%; Figure 2C). This is clearly shown in Figure 2A, where the majority of $D1^+$ neurons in the SGS are yellow and the bulk of $D1^+$ $VGAT^+$ cell density is in the SGS. Figure 2A (right) shows a high-magnification image of the D1-tdTom × VGAT-Venus SGS, where nearly every $D1^+$ cell imaged in the SGS is $VGAT^+$. Figure 2C shows a scatterplot illustrating that D1 co-localization with VGAT is correlated with depth from the dorsal SC surface. Below the dorsal-most 400 μm of the SC, D1 neurons no longer preferentially co-localize with VGAT (Figure 2C). This change was statistically significant ($p < 0.0001$), as the average depth of a $D1^+$ $VGAT^-$ neuron was significantly more ventral than $D1^+$ $VGAT^+$ cells (Figure 2D; average depths: 229.58 μm $D1^+$ $VGAT^+$, 380.34 μm $D1^+$ $VGAT^-$).

Contrary to the primarily inhibitory nature of $D1^+$ neurons, 63% of $D2^+$ neurons were $VGAT^-$ while only 37% were $VGAT^+$ (Table 1; Figure 2B). D2 co-localization with VGAT, unlike D1, was uniform across the depth of the SC at ~30%–40% (Figure 2C), and the average depth of $D2^+$ cells expressing VGAT versus those not expressing VGAT did not reach statistical significance (Figure 2D).

D2 Islands

$D1^+$ and $D2^+$ neurons maintained the same laminar segregation and excitatory/inhibitory identity across the rostro-caudal axis (Figure S1; Table 1). However, a unique feature of the rostro-medial SC, which is known to map ventro-temporal retina, were clusters of ~30 $D2^+$ neurons per confocal optical section (Sperry, 1963). These clusters, which we call "D2 islands," were localized within the SC commissure where the two SC hemispheres begin to connect at the midline and communicate through cross-collicular projections (Figure S2A). Interestingly, nearly all D2 island cells counted (56/59) were negative for VGAT (n = 2 D2-tdTom × VGAT-Venus rostral slices from two different animals; Figure S2B).

Dopamine Source to the SC Is Primarily DAT^-

We next sought to characterize the source of SC dopamine using retrograde labeling. The SCs of seven mice (five wild-type [WT] mice and two DAT-IRES-Cre knockin mice crossed to the floxed-tdTomato reporter line [DAT-tdTom]) were stereotaxically injected with latex microspheres that travel retrogradely along axons (Retrobeads, Lumafluor). Serial sections were prepared, and each sample was stained with antibodies for the dopamine synthesizing enzyme tyrosine hydroxylase (TH) and the dopamine transporter (DAT), which is known to re-uptake dopamine into presynaptic terminals after dopamine release. TH catalyzes the conversion of tyrosine to the required dopamine precursor L-DOPA and is therefore only present in neurons capable of dopamine production. However, because dopamine can be converted to norepinephrine or epinephrine in hindbrain cell groups (A1–A7, the locus coeruleus, and C1–C3: Mejías-Aponte et al., 2009), TH marks all dopamine, norepinephrine, and epinephrine neurons. DAT, on the other hand, is thought to only demark dopamine-releasing cells (Fu et al., 2012; Tritsch et al., 2012; Tecuapetla et al., 2010). DAT co-localizes with TH at close to 100% in ventral midbrain dopamine neurons and is found in every known dopaminergic cell group except group A13 in the diencephalon, which is critical for this report (Fu et al., 2012; Tritsch et al., 2012). We first focus on the dopaminergic axons within the SC and next show that the TH^+ axon pattern in the SC corresponds perfectly to the pattern of retrogradely labeled TH^+ neurons.

In all of our samples, TH^+ axons were extremely dense in the SC (Figure 3A, left), with no preferential targeting to specific SC layers. This means that axons capable of producing dopamine terminate broadly in the mouse SC, which has been observed in other species (Mooney et al., 1990; Arce et al., 1994; Metzger et al., 2006). DAT-tdTom reporter (Figure 3A, center) and DAT antibody staining (Figure 3A, right), on the other hand, were sparse or nearly absent in SC axons, respectively, although both DAT-tdTom and DAT immunohistochemistry (IHC) were highly coexpressed in the ventral midbrain in the exact same slices, and show full co-localization in the same samples in the basal ganglia (Figure S3). DAT IHC stained an average of only 7.5 axons per SC slice (4 DAT IHC-stained SC slices counted; Figure 3A, right) compared to the thousands of TH^+ axons observed in the SC. Additionally, nearly all DAT-$tdTom^+$ terminals found within the SC were TH^- (502/520 DAT^+ axon endings were TH^-, n = 7 slices across three animals; Figure 3B), meaning that these axons arise from DAT-tdTom-expressing neurons that are incapable of synthesizing dopamine. This was not typical as both ventral midbrain in the same slices and basal ganglia in the same samples show that DAT-tdTom- and DAT-IHC-expressing axons overlap robustly with our TH antibody (Figure S3).

The expression pattern of TH, DAT-tdTom, and DAT IHC agreed fully with the pattern of retrobeads observed in the seven injected animals. A typical retrobead injection into the SC is

shown in Figure 3C. Retrobeads transported retrogradely from SC injection sites were consistently observed in only two TH^+ cell groups in all seven animals, and both labeled groups were DAT^-. The first group is the locus coeruleus (LC), a canonical noradrenergic hindbrain region previously shown to project strongly to the superficial SC (Arce et al., 1994; Figure 3D). It has been recently demonstrated that the locus coeruleus can co-release dopamine, which provides a possible basis for dopamine receptor activation in the SC (Devoto et al., 2005a, 2005b).

The second retrogradely labeled TH^+ region is the A13 cell group of the zona incerta (Figure 3E). As noted, this cell group is known as the only DAT^-, TH^+ dopamine cell group in the brain (Tritsch et al., 2012). All seven injections showed retrograde labeling of A13, which never stained positive for DAT antibody nor showed DAT-tdTomato expression (Figure 3E; note DAT and TH antibody co-stained axons, typical of midbrain dopamine projections, right next to A13, running from midbrain to the caudate putamen).

Midbrain dopamine neurons were practically devoid of retrobeads in all animals studied (two total DAT^+, TH^+ neurons found in seven animals). No clear retrogradely labeled neurons were observed in any of the three major midbrain dopamine cell groups [the retrorubral field (A8), the substantia nigra pars compacta (A9), and the ventral tegmental area (A10)], which all stained for DAT and showed DAT-tdTom reporter expression (Figure S4). A previous line of research suggested that dopamine neurons coexpressing GABA in the substantia nigra pars reticulata (SNr) project to the SC in the rat (Campbell et al., 1991). Retrobeads were found consistently in all samples in TH^- neurons of the substantia nigra pars reticulata (SNr; Figure S4), which likely represent the GABAergic projection found by Hikosaka and Wurtz (1985) that tonically inhibits the SC. However, we never observed any retrograde labeling of TH^+ neurons in the SNr. It is possible that our retrobead injections were simply not taken up by terminals described by Campbell et al. or that our injections were not in the same locations within the SC.

We also managed to identify why DAT-tdTom$^+$ axons in the superficial SC do not stain for TH (Figure S5). A small packet of hindbrain neurons lying just underneath the fourth ventricle was retrogradely labeled in both DAT-tdTom mice tested. These neurons lacked TH (Figure S5A) and were not stained by the DAT antibody (Figure S5B), indicating a lack of dopaminergic identity in the adult animal. Due to the DAT reporter being an IRES-Cre, DAT was likely expressed in this cell population at some point during development. Whether this population ever expressed TH or provided dopamine to the SC is unknown.

Dopamine Alters Electrophysiology of D1 and D2 Neurons

Patch-clamp electrophysiology was used in acute sagittal SC slices to determine how $D1^+$ and $D2^+$ cells may respond to dopamine released from A13 or the LC. $D1^+$ neurons in the SGS were current clamped while their afferent visual axons in the SO were electrically stimulated to mimic visual input. Stimulation intensity was increased until each delivered stimulus evoked a spike in the postsynaptic $D1^+$ cell (Figure 4A). When dopamine (50 μM) was washed onto the slice, these evoked spikes were eliminated in 12/14 cells tested (11 complete spike elimination, 1 partial with 18/31 failures, 2 no reduction: average 1 spike/stimulation control versus 0.18 spikes/stimulation DA, $p < 0.0001$; Figure 4A). Spike failures began on average 52.65 s (± 27.11 s) after initiation of dopamine wash-in, occurred independently of resting voltage shifts (4 cells show an increase in V_m with dopamine whereas 8 cells show a decrease; $p > 0.05$), and were completely reversible after dopamine washout in 10 out of 12 cells. Of the 14 cells tested, 3 out of 3 pre-bathed with gabazine (20 μM) showed full spike elimination upon dopamine wash-in, suggesting that despite $D1^+$ cells being ~70% GABAergic in the SGS, spike elimination was not due to an indirect increase in GABAergic inhibition. Furthermore, in voltage-clamp experiments (−70 mV holding voltage, Mg-containing artificial cerebrospinal fluid [ACSF], 20 μM gabazine), dopamine reduced compound excitatory post-synaptic currents (EPSCs) evoked by SO stimulation by an average of 65% ($p < 0.01$, $n = 9$; Figures 4B and 4D), suggesting that spiking was eliminated because EPSCs were incapable of driving the neurons to spike threshold.

Interestingly, spike elimination in response to SO stimulation was not replicated by the D1 agonist SKF81297 (10 μM, $n = 4$ cells, 3 no spike reduction, 1 temporary resting drop that rebounded after 132 s) or the D2 agonist quinpirole ($n = 2$ cells, no reduction). Instead, the main effect of SKF81297 wash-in appeared to be a reduction in GABAergic inhibition among the network of $D1^+$ GABAergic SGS neurons. Spontaneous inhibitory post-synaptic currents (IPSCs) were recorded in six $D1^+$ SGS cells (voltage clamp at +30 mV, NBQX [10 μM], AP5 [25 μM] in bath). Five cells showed a reduction in average IPSC amplitude, while four showed a reduction in IPSC frequency 2 min after SKF81297 washin. The most prominent effect on IPSCs, however, appeared after the washout of SKF81297. SKF81297 washout induced a rebound effect on IPSC frequency in all cells that maintained constant seal during 5 min of washout (5/5, $p < 0.05$, Wilcoxon signed rank test; Figures 4C and 4D). On average, there were 29% more IPSCs recorded 5 min after SKF81297 washout than during SKF81297 incubation, which can be clearly seen in two representative cells in Figure 4C.

Next, $D2^+$ neurons in the intermediate layers were current clamped to read out raw resting voltage. When dopamine (50 μM) was washed into the bath, resting potential decreased on every neuron tested, sometimes severely (up to 14 mV shifts, 4.31 mV mean decrease, $n = 14$ cells, $p < 0.001$, Figures 5A and 5D). In a subset of neurons, equivalent injected current ramps were performed in control and dopamine conditions. Dopamine exposure significantly decreased spiking during current ramps as seen in Figure 5A (mean drop of 15.06 spikes per ramp, $p < 0.05$, $n = 8$, Figure 5D, right). Moreover, in 2/2 neurons where spontaneous network firing was observed in control conditions, dopamine washin remarkably silenced spontaneous firing (Figure 5C), indicating that dopamine has a strongly depressive influence over the SC circuit. The D2 antagonist sulpiride (10 μM) was effective in blocking the resting shift induced by dopamine ($n = 4$, −0.8 mV shift, $p = 0.167$; Figures 5B and 5D); furthermore, with all synaptic conductances blocked (20 μM gabazine, 10 μM NBQX, Mg-ACSF for NMDAR), the D2 agonist quinpirole (10 μM) was highly effective at replicating the resting shifts (drop on all cells tested, −2.67 mV average, $n = 7$, $p < 0.05$;

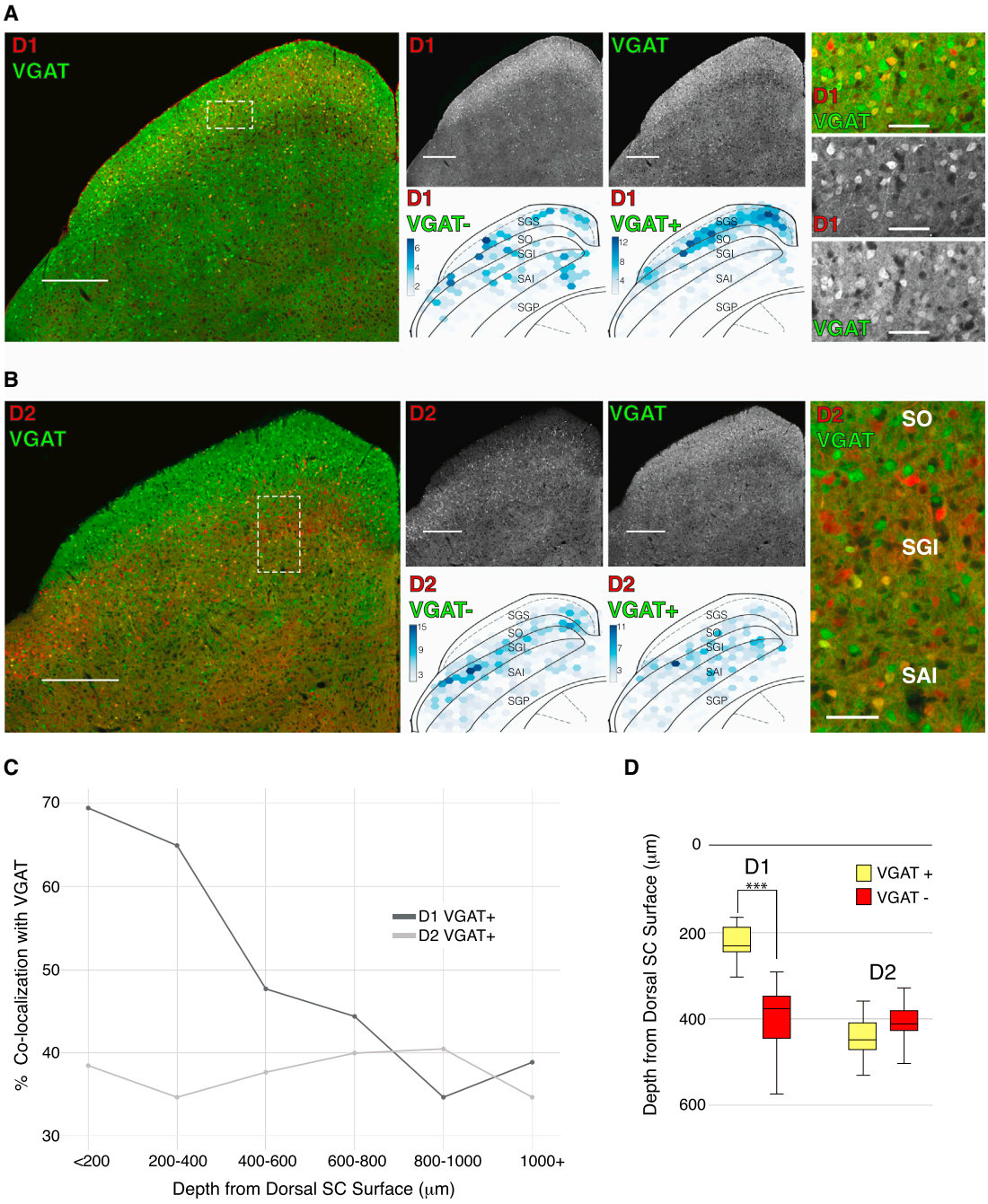

Figure 2. D1 Neurons in the SGS Are Primarily Inhibitory, while D2 Neurons Are Mostly VGAT$^-$

(A and B) D1-tdTom mice (A) and D2-tdTom mice (B) were crossed to a line expressing the yellow fluorescent protein Venus under the *Vgat* promoter. D1-tdTom neurons in the SGS co-localized strongly with VGAT, as illustrated by the high density of D1$^+$ VGAT$^+$ cells in the SGS in the 2D histogram and the zoomed image in the rightmost panels (representing the area inside the white dashed box on the leftmost panel). D2-tdTom cells, on the other hand, were primarily negative for VGAT. The highest density bins for D2$^+$ VGAT$^-$ cells were in the upper SGI (shown in zoomed image and histogram), while density of D2$^+$ VGAT$^+$ bins was spread throughout the SGI and SAI, leading to a slightly deeper average depth for D2$^+$ VGAT$^-$ cells (2D). Total numbers of cells counted across three animals are reflected by bin color according to legends left of each panel. Scale bars represent 300 μm on full SC images and 50 μm on rightmost zoomed images. Hexagons are 80 μm wide in histograms.

(C) Scatterplot displaying percent co-localization of D1$^+$ and D2$^+$ neurons with VGAT, binned according to depth from the dorsal SC surface. D1$^+$ neurons expressed VGAT far more commonly in the most superficial SC (0 to 200 μm bin), where ~70% of cells were VGAT$^+$. This percent overlap of D1 with VGAT decreased with depth from the SC surface. There was no apparent change in VGAT co-localization with D2 across the SC layers.

(D) Boxplot illustrating the distribution of median depths of D1$^+$ VGAT$^+$, D1$^+$ VGAT$^-$, D2$^+$ VGAT$^+$, and D2$^+$ VGAT$^-$ neurons from the dorsal SC surface. Median depths were calculated in each slice (rostral, middle, and caudal) of three D1-tdTom × VGAT-Venus and three D2-tdTom × VGAT-Venus samples. D1$^+$ neurons

(legend continued on next page)

Figures 5B and 5D), indicating that resting drops induced on $D2^+$ neurons are cell autonomous and D2 dependent. We therefore conclude that the primary action of dopamine on D2 neurons of the intermediate layer is to reduce resting potential, thereby hampering the cell's ability to fire in response to excitatory currents induced by injection or network activity.

DISCUSSION

Responses of neurons in the SC are modulated by current behavioral demands of the animal (Felsen and Mainen, 2012; Ikeda and Hikosaka, 2003, 2007; Basso and Wurtz, 1998). Our characterization of the anatomy, gene expression profile, and electrophysiological consequences of the dopamine input to the SC lays the groundwork for understanding how A13 and dopamine receptor activation within the SC may modulate SC-mediated behaviors.

We began our study by using transcriptome analysis, showing that *Drd1* and *Drd2* are the only two dopamine receptors that are strongly expressed in the SC (Figure 1B). Cells expressing these receptors were then localized within the layered SC structure. $D1^+$ cells were enriched in the "visual map" of the SGS, where D1 strongly co-localized with VGAT. D1 localization to the superficial SC is supported by previous in situ and D1 agonist binding studies (Mansour et al., 1992; Mengod et al., 1991). $D2^+$ cells, on the other hand, were dense in the intermediate layer "motor map" and tended to be non-GABAergic (Figures 1 and 2).

As previously noted, dopamine is present at higher concentrations in the SC than in either the hippocampus or frontal cortex (Versteeg et al., 1976). The dopamine-synthesizing enzyme TH shows dense axonal expression in the mouse SC (Figure 3), as has also been seen in other species (Arce et al., 1994; Metzger et al., 2006; Mooney et al., 1990). Moreover, previous studies have shown that the COMT-generated dopamine breakdown product 3-MT, which does not arise after norepinephrine or epinephrine breakdown by COMT, is found in the SC at the same order of magnitude as the striatum (Weller et al., 1987), again suggesting a significant dopamine input to the SC. Our retrograde tracing results support a role for A13 and possibly the LC in providing this dopamine to the SC, and our RNA-seq and IHC results, coupled to other's findings, hint at how this dopamine may be recycled and metabolized. Specifically, the fact that 3-MT is highly concentrated in the SC is not surprising considering we found abundant *Comt* mRNA in the SC and a means for COMT and MAO to access dopamine via PMAT (Figure 1B). Moreover, the dopamine transporter, which clears dopamine from synapses for reuse and does not generate 3-MT, was nearly undetectable in the SC using DAT IHC, a DAT reporter line (Figure 3), and RNA-seq (Figure 1B). This lack of DAT expression supports previous data showing that dopamine reuptake by axons does not occur in the SC (Weller et al., 1987) and was the initial indicator that the primary source of dopamine to the SC is not the DAT-expressing midbrain dopamine centers (A8, SNc, and VTA) traditionally associated with dopamine function (Schultz, 2007). The fact that dopamine breakdown appears to be the only mode of dopamine clearance in the SC is important for future studies considering that COMT-generated dopamine breakdown products like 3-MT and homocysteine can modulate synaptic conductances (Bolton et al., 2013; Sotnikova et al., 2010).

TH^+ axons in the superficial hamster SC were previously shown to co-localize with dopamine beta-hydroxylase (DBH), the norepinephrine-producing enzyme, at a 92% rate. This previous study determined the locus coeruleus as the primary source of the DBH^+, TH^+ projection to the superficial SC (Arce et al., 1994), which is consistent with our retrograde labeling of the LC in all injected mice. We surmise that the remaining 8% of TH^+, DBH^- axons in the SC are from the dopamine cell group A13, the only other ubiquitously labeled TH^+ cell group found in our retrograde experiments. A recent line of research has found that dopamine is co-released with norepinephrine from locus coeruleus terminals, meaning that both A13 and the LC could be the SC dopamine source (Devoto et al., 2005a, 2005b). Moreover, a second line of research describes the promiscuity of dopamine receptors regarding which catecholamine activates them. Norepinephrine, for example, can activate D2 receptors (Onali et al., 1985; Odagaki et al., 1995; Lanau et al., 1997; Johnston et al., 2001) and in doing so can modulate HCN currents (Arencibia-Albite et al., 2007). It may therefore be possible that the locus coeruleus *does* only release norepinephrine from its TH^+ SC terminals but that this norepinephrine can activate D2 dopamine receptors in the SC. Moreover, recent evidence has shown the opposite scenario: dopamine can activate norepinephrine receptors (Cilz et al., 2014), which could explain why the D1 agonist SKF81297 did not mimic dopamine's ability to reduce evoked spiking in $D1^+$ cells.

How might the arrangement of dopamine axons and receptors in the SC affect behavior? The depressive effects of dopamine on $D2^+$ cells were often severe (sometimes reaching 14 mV drops; Figure 5A), reducing the ability of $D2^+$ neurons to spike during current injection (Figures 5A and 5D). Under such conditions, dopamine would practically shut down $D2^+$ SC neurons, which are primarily non-GABAergic and lie in the SC layer where excitatory neuron activation induces orienting behaviors and attention shifts (e.g., Robinson, 1972; Müller et al., 2005; Northmore et al., 1988; Ewert, 1984). The inhibition of retina-driven EPSCs by dopamine and the reduction of $D2^+$ neuron firing resemble the dampening of visual responses and the silencing of the intermediate layer in the toad tectum by dopamine receptor activation (Glagow and Ewert, 1997, 1999); these physiological effects resulted in a phenotype where the toad no longer oriented or attended to prey items. Future experiments could address whether A13 activation results in this type of "waiting behavior." Considering that neurons in the intermediate SC have visual, auditory, and somatosensory receptive fields (Huerta and Harting, 1984b), and that the intermediate SC can

expressing VGAT were significantly superficial to $D1^+$ cells that were negative for VGAT (***$p < 0.0001$). $D2^+$ neurons, however, showed similar locations whether they expressed VGAT or not, with the average depth of $D2^+$ $VGAT^+$ neurons (447.82 μm) slightly below $D2^+$ $VGAT^-$ cells (410.86 μm) without reaching statistical significance ($p = 0.055$, right boxplots). Ends of whiskers are maximum and minimum of the distributions, box edges are first and third quartiles, and lines inside boxes are medians.

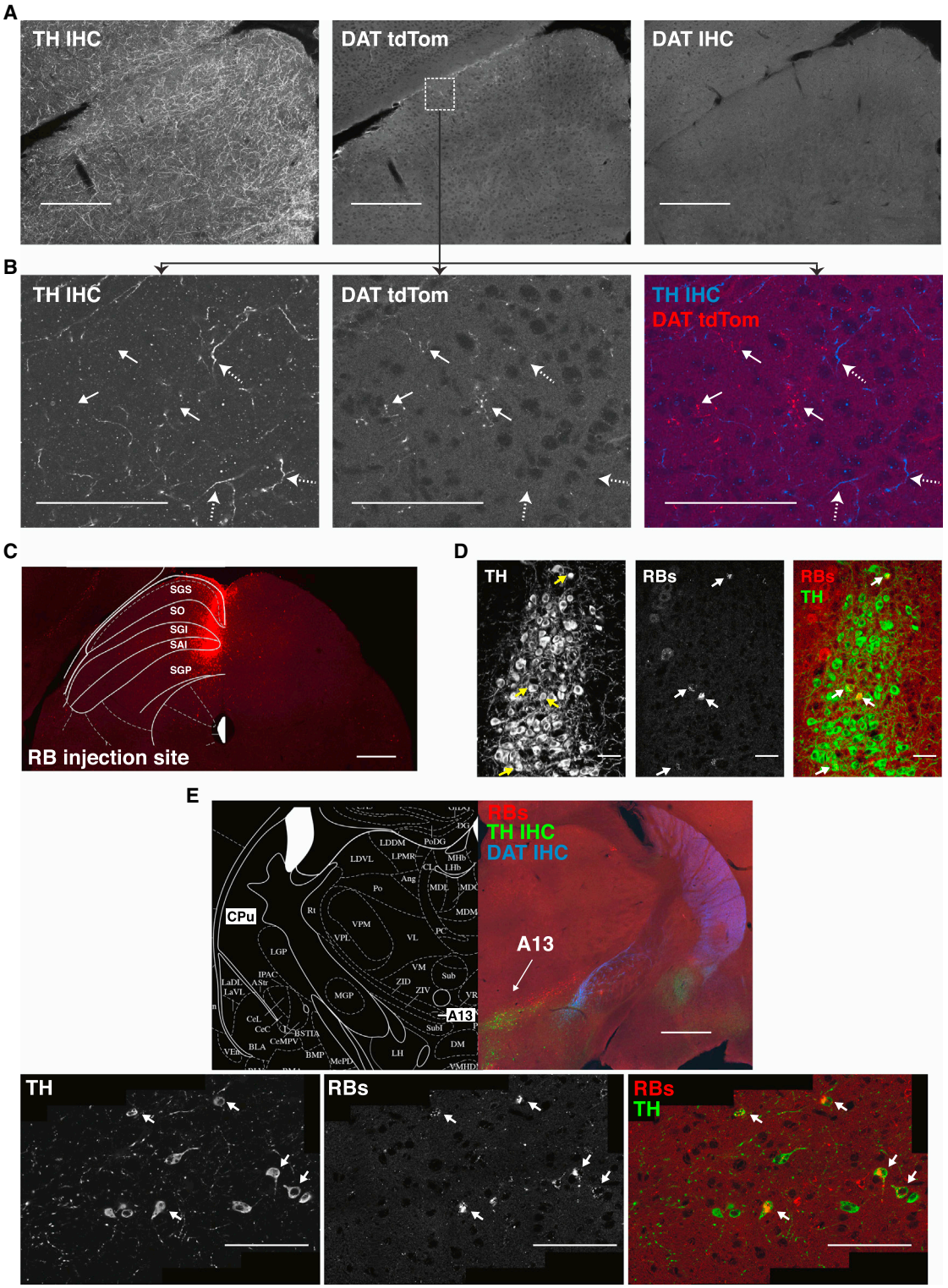

Figure 3. Dopamine-Producing Axons Are Present in the SC, but DAT Is Sparse, and DAT Reporter Does Not Localize to TH$^+$ Elements

(A and B) TH IHC reveals dense termination of catecholaminergic axons in the SC (A, left). However, DAT-tdTom (A, center) and DAT IHC (A, right) were sparse or absent, respectively. The sparse DAT-tdTom-expressing terminals found in the superficial SC did not co-localize with TH (B), suggesting that these axons arrive from cells that are non-dopaminergic in the adult mouse (TH IHC and DAT-tdTom are on the same slice, and DAT IHC is one serial slice later). Scale bars represent 300 μm (A) and 50 μm (B).

(legend continued on next page)

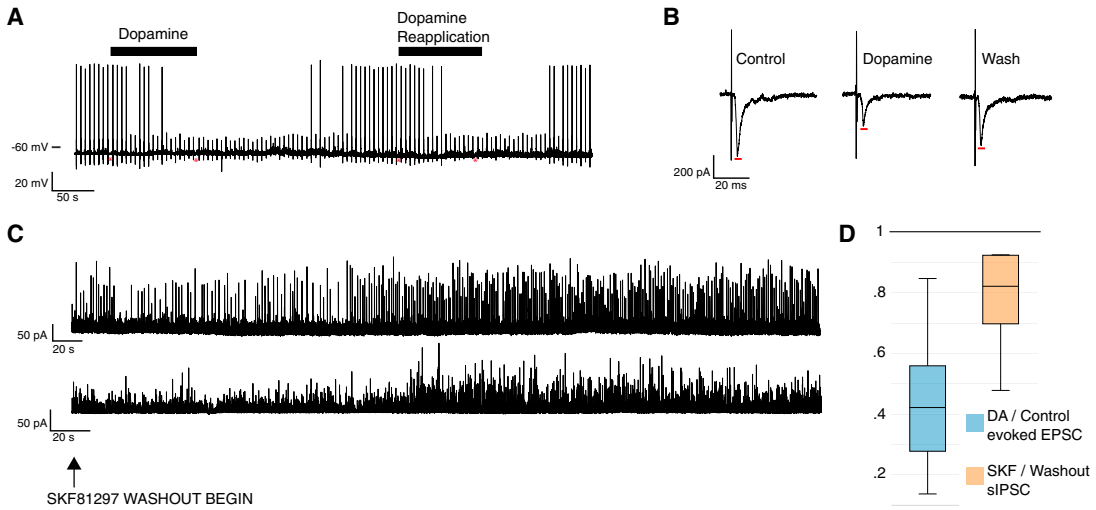

Figure 4. Electrophysiological Effects on D1$^+$ SC Neurons

(A) Spikes were evoked in D1$^+$ neurons by SO stimulation to mimic visual input. Stimuli were applied every 5 s in current clamp; dopamine washin eliminated spiking in most cells tested (11/14) and partially eliminated spiking in an additional cell (18/32 failures). These effects were completely reversible in 11 cells. Red stars indicate brief pauses in the electrophysiological record to test seal and access resistance.

(B) EPSCs evoked by SO stimulation were significantly reduced (average 65% reduction, n = 9 cells) by dopamine, measured after 2 min of dopamine exposure. Again, this effect was reversible.

(C) Although SKF81297 did not replicate dopamine's effect on spike elimination, this D1 agonist did affect amplitude and frequency of spontaneous IPSCs (+30 mV holding, NBQX [10 μM], AP5 [25 μM] in bath). This was especially clear during SKF81297 washout (shown here in two different neurons), where IPSC frequency significantly increased in all five cells tested.

(D) Boxplot showing the complete distribution of percentage drops for evoked EPSCs (dopamine/control) and spontaneous IPSCs (SKF/washout). Ends of whiskers are maximum and minimum of the distributions, box edges are first and third quartiles, and lines inside boxes are medians.

project back to and influence responses in the SGS (Vokoun et al., 2010; Phongphanphanee et al., 2011), it will be interesting to see whether D2 activation specifically affects particular modalities or particular feedback circuits.

Although it appears that dopamine is primarily inhibitory to SC neurons, dopamine's effect on neural circuit function is likely complex considering that D1$^+$ and D2$^+$ populations both co-localize with VGAT to some degree (Figure 2) and that electrophysiological effects on these inhibitory cells were noted using D1 agonists (Figure 4). To understand how dopamine truly influences the SC, it is critical to discover how A13 responds during tasks typically thought to require dopamine. Although the dopamine architecture described in this study could be responsible for the modulation of SC activity by reward (Ikeda and Hikosaka, 2003, 2007), A13 may be involved in tasks not normally ascribed to dopamine. Moreover, it will be critical to understand dopamine's role in the SC within the context of brain-wide dopamine signaling. Neurons in the striatum, for example, receive a large dopamine projection from the midbrain and express D1 or D2 receptors on nearly every cell (Thibault et al., 2013). The direct effects of dopamine on the SC may therefore be less significant than indirect effects of dopamine on neurons efferent to the SC. However, we believe the direct behavioral effects of dopamine on the SC will prove to be important considering that our electrophysiological findings on D2$^+$ neurons were cell autonomous (Figure 5; all synaptic conductances blocked on quinpirole experiments) and the fact that D1 and D2 receptors are expressed on the order of two of the most common and fundamental glutamate receptor transcripts in the brain (Figure 1).

In conclusion, we believe our study lays a genetic, anatomical, and electrophysiological foundation for the future exploration of dopamine in the SC. Linking behaviorally relevant dopamine neuron activity in A13 to dopamine release and D1$^+$/D2$^+$ cell modulation in the SC should be the primary goal of future research in this area, which should hopefully explain how the laminar arrangement of D1 and D2 cells relate to the SC's role in attention and sensorimotor transformations during orienting.

EXPERIMENTAL PROCEDURES

All experiments were carried out with the approval of the Committee on Animal Care at the Massachusetts Institute of Technology.

(C) Typical injection site of retrobeads, restricted to the SC.

(D) Retrobeads (center, right) transported from the SC co-localize with TH$^+$ neurons (left) in the locus coeruleus.

(E) TH$^+$ neurons in A13 (top, bottom left), a DAT$^-$ region in the zona incerta, are consistently labeled with retrobeads from the SC (top, bottom middle, right). Note the DAT$^+$ terminals emanating from the SN/VTA that run laterally to A13 toward the basal ganglia. Scale bars represent 300 μm (C), 100 μm (D), 300 μm (E, top), and 50 μm (E, bottom).

Bottom panels are composites of eight 60× images taken in A13 stitched together with Nikon NIS-Elements.

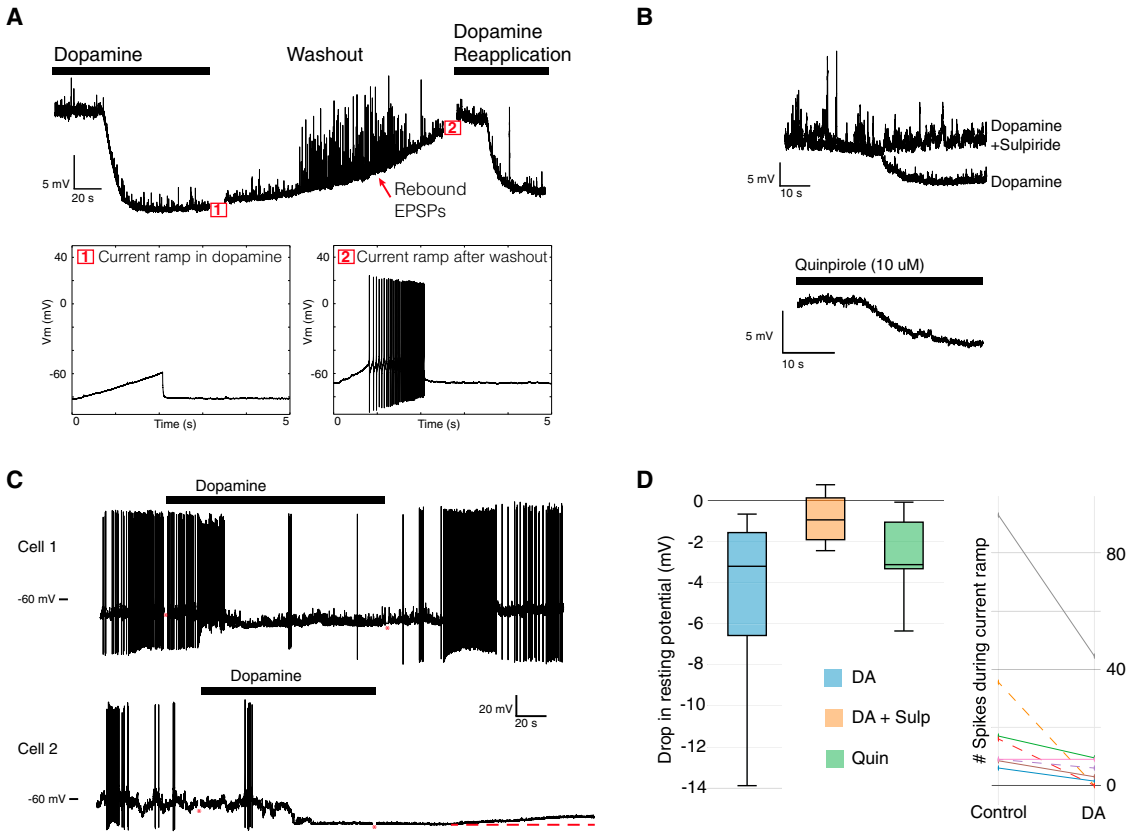

Figure 5. Electrophysiological Effects on D2$^+$ SC Neurons

(A–C) Dopamine application (50 μM) to current clamped D2$^+$ neurons in the intermediate SC reduced resting voltage on all cells tested (n = 14) (A). This often severe effect of dopamine washin significantly reduced spiking during injected current ramps (1 and 2) (A and D) and robustly eliminated spontaneous network firing in two cells where spontaneous spiking was observed (C). The D2 agonist quinpirole (10 μM) also reduced resting voltage in all cells tested (n = 7) and resting drops induced by dopamine were blocked by the D2 antagonist sulpiride (10 μM) (B).

(D) Left: boxplot showing the distribution of resting voltage drops in response to dopamine, dopamine and sulpiride, and quinpirole. Ends of whiskers are maximum and minimum of the distributions, box edges are first and third quartiles, and lines inside boxes are medians. Right: each color represents a D2 cell where equivalent current ramps were injected into the neuron both in control conditions and during dopamine exposure. Solid lines indicate that spikes were taken first in control ACSF and second in dopamine ACSF, and dotted lines indicate that spikes were recorded first in dopamine ACSF and second after washout to control ACSF, ruling out order-related effects. Red stars in (C) indicate brief pauses in the electrophysiological record to test seal and access resistance.

Animals

Mice listed as WT are C57B6/J. Strains from GENSAT include D1-Cre (FK150), D2-Cre (ER44), and D2-EGFP (S118). D2-EGFP mice were backcrossed to C57B6/J after arriving on a Swiss Webster background. Strains from Jackson Laboratory include D1-tdTomato (#016204), floxed-tdTomato (#007914), DAT-Cre (#006660), and TH-Cre (#008601). VGAT-Venus mice were generously given to us by Janice Naegele (Wang et al., 2009). Venus was developed by Dr. Atsushi Miyawaki at RIKEN (Wako).

RNA-Seq

Total RNA from the 3-week-old rat superior colliculus was extracted using Qiazol (QIAGEN) reagent according to the manufacturer's instructions. Total RNA was cleaned up using the RNeasy MinElute kit (QIAGEN) and stored at −80°. The purity of RNA was assayed using a NanoDrop, and samples with 260/280 ratios less than 1.8 or 260/230 ratios less than 2.0 were subjected to a second round of cleanup and discarded if they were still not pure after the second cleanup. Samples were run on the Agilent 2100 Bioanalyzer and samples with RIN numbers less than 9 were discarded. Samples were stored at −80° until library creation.

DNA libraries for paired-end sequencing on the Illumina Genome Analyzer II were prepared following the Illumina protocol (#1004898 Rev. D) with a few alterations. The resulting product was PCR amplified for ten cycles using primers against the Illumina adaptors. The final library was run on an Agilent Bioanalyzer to confirm proper size selection. Samples were submitted to the BioMicro Center at MIT for sequencing on the Illumina Genome Analyzer II with 36-bp paired-end reads.

We processed the RNA-seq data using the best-practice RNA-seq pipeline implemented in version 0.7.9a of the bcbio-nextgen framework. In brief, we trimmed off poor-quality ends with AlienTrimmer version 0.3.2, using a cutoff of a phred score of 5 or less, and trimmed portions of reads and anything after it matching the first 13 bases of the Illumina universal adaptor sequence to remove read-through contamination caused by the read length being longer than the insert size for a fragment. We also trimmed polyA and polyT homopolymer sequences from the 5′ ends of reads. Reads were aligned using the STAR aligner version 2.3.14z against the *rattus norvegicus* genome build rn5 and Ensembl release 74 of the gene annotation. Counts of reads mapping to genes in the Ensembl annotation were calculated using FeatureCounts version 1.4.4 and FPKM expression was estimated using Cufflinks version 2.1.1.

Animal Surgery

Postnatal day 10 (P10) to P16 mice were anesthetized with isoflurane and immobilized in a stereotaxic frame. The skin overlying the skull was incised and a

dental drill was used to burr a hole though the skull above the SC. Glass pipettes (Drummond) were pulled and ~2 μl latex microspheres (Retrobeads IX, Lumafluor; green beads were injected at 100% and red beads injected at 25% beads:PBS) were loaded into the pipette tip using a Drummond Nanoject. Loaded pipettes were lowered under stereotaxic guidance into the SC. Microspheres were injected (~45–100 nl total), and the pipette was slowly retracted 5 min later. Animals were sutured and returned to their home cages for ~2 weeks before perfusion.

Anatomy and Histology

Animals were perfused through the heart with 15 ml PBS followed by 15 ml 4% paraformaldehyde in PBS under isoflurane anesthesia. Brains were extracted and post-fixed in 4% paraformaldehyde at 4°C overnight. After post-fixing, brains were transferred to 30% sucrose in PBS for cryoprotection at 4°. Slices were cut at 75–90 μM using a Leica freezing microtome or a Leica cryostat with OCT as a freezing medium. For IHC, free-floating slices were incubated for ≥2 hr at room temperature in a blocking buffer containing 1% Triton X-100 and 5% goat or donkey serum in PBS. Slices were then incubated on a shaker overnight at 4° in blocking buffer containing primary antibody. Primary antibodies used included rabbit anti-tyrosine hydroxylase (Millipore AB152; 1:1,000), rat anti-DAT (Millipore MAB369; 1:1,000), rabbit anti-RFP (MBL PM005; 1:2,000), chicken anti-GFP (Abcam ab13970; 1:10,000), and mouse anti-NeuN (Millipore MAB377; 1:3,000). After primary antibody incubation, slices were washed in PBS for 15 min three times. Slices were then incubated in Alexa-conjugated immunoglobulin G (1:500 or 1:1,000) directed to the species of the primary antibody in blocking buffer at room temperature for 2 hr. After a second round of three 15 min PBS washes, slices were mounted with Fluoromount. All samples were imaged using a Nikon C2 confocal system equipped with 488 nm, 561 nm, and 647 nm lasers. A 20× Nikon Plan Apo objective was used for most images, while a Nikon 60× Plan Apo Oil objective was used for high-magnification imaging. Images in figures were edited in Adobe Photoshop using the autocontrast function, and brightness was enhanced in some cases for display purposes. All axon and cell counting was performed on raw images.

Cell Counting

Custom software for counting and assigning coordinates to fluorescent neurons was written in Python by A.D.B. This software with instructions is freely available at http://github.com/LarryLegend33. Heatmap histograms were created using Python Matplotlib's "hexbin" function with a minimum count of 1 (i.e., bins with 0 or 1 counts appear as white). Histograms were overlaid with atlas pictures from Paxinos' *Mouse Brain in Stereotaxic Coordinates*. Samples chosen for cell counting came from three coronal planes of the SC. Caudal samples were ~4.4 mm caudal to bregma, rostral samples were ~3.4 mm caudal to bregma, and middle slices were approximately halfway between the chosen caudal and rostral slices (Paxinos' *Mouse Brain in Stereotaxic Coordinates*). The dorsal surface of each SC slice was traced using our cell-counting software; points along the dorsal surface served as a reference for calculating cell depth within the SC structure. Dorsal surface traces included the full medial-lateral expanse of the SC from the midline SGS to the lateral-most SGI, terminating when the tracing line became vertical. Median depths of each neuron type were calculated for each slice in each sample, and t tests were used to compare the distributions of these average depths between cell groups (e.g., Figures 1E and 2D).

Slice Electrophysiology

P20–P45 mice were anesthetized in a bell jar using isoflurane and decapitated (D2-tdTom, D2-EGFP, D1-tdTom, and D1-Cre × Flox-tdTom). The brain was quickly removed and submerged in an ice-cold sucrose cutting solution containing 206 mM sucrose, 2.5 mM KCl, 1.2 mM NaH_2PO_4, 24 mM $NaHCO_3$, 5 mM HEPES, 12.5 mM glucose, 0.4 mM sodium ascorbate, 10 mM $MgSO_4$, and 0.5 mM $CaCl_2$. After 1 min of cooling, the brain was mounted on a Leica vibratome and submerged in sucrose solution. Before slicing, the brain rostral to the SC was dissected off and the rhombencephalon caudal to the inferior colliculus was removed. Sagittal SC slices, containing the full dorsal-ventral expanse of the midbrain only, were prepared at 280 μm. Slices were then incubated at 32° for 15 min in a carbogenated slice chamber filled with ACSF composed of 124 mM NaCl, 2.5 mM KCl, 1.2 mM NaH_2PO_4, 24 mM $NaHCO_3$, 5 mM HEPES, 12.5 mM glucose, 0.4 mM sodium ascorbate, 2 mM $MgSO_4$, and 2 mM $CaCl_2$. The chamber was then removed from the 32° water bath and allowed to return to RT. Slices recovered for at least 1 hr before being added to a recording chamber under continuous perfusion of ACSF (~2 ml/min). For voltage clamp, pipettes were filled with a solution containing 105 mM Cs-gluconate, 10 mM phosphocreatine (Na), 0.07 mM $CaCl_2$, 4 mM EGTA, 10 mM HEPES, 4 mM Na-ATP, 1 mM Na-GTP, and 3 mM $MgCl_2$, brought to osmolarity of ~290 mOsm with sucrose. In some experiments, sucrose was omitted and neurobiotin (0.5%) was used. Current clamp internal solution was identical except 105 mM K-gluconate replaced Cs-gluconate. Cells were patched with glass pipettes (Sutter) pulled to 3–7 MΩ using a Multiclamp 700B with pClamp10 software or an Axopatch 1D with pClamp8, sampling at 20 kHz and filtering at 2–10 kHz. Cells recorded in current clamp were rejected if resting voltage after breakin was greater than −50 mV. Fast bath exchange (~10 s until arrival of drug) was performed using an ALA VM-4 perfusion system with a Millimanifold attached directly to the bathing chamber, with the bath kept at ~30°C–32°C. Neurons were visualized before patching with an Arclamp and identified as $D1^+$ or $D2^+$. For experiments stimulating the SO, a concentric bipolar electrode (FHC) driven by a World Precision Instruments IsoStim 320 was placed in the SO axons at the rostral pole of the SC. Stimulating intensities were raised until spikes were driven in the post-synaptic neuron. Typical current applied was ~0.1 mA. Data were analyzed using Clampfit (Axon Instruments) and MiniAnalysis (Synaptosoft). Resting voltages in D1 and D2 experiments were calculated in Clampfit using the "mean" calculation in the Statistics suite over a 10 s window. For D1 EPSCs, amplitudes of currents evoked every 5 s were averaged in a 30 s windows before, exactly 120 s after DA washin, and an average of 5 min after washout (average 300.77 s). Paired two-tailed t tests were used as significance tests (unless noted).

ACCESSION NUMBERS

The accession numbers for the gene expression data reported in this paper are GEO: GSM1872016, GSM1872017, GSM1872018 (http://www.ncbi.nlm.nih.gov/geo/query/acc.cgi?acc=GSE72787).

SUPPLEMENTAL INFORMATION

Supplemental information includes five figures and can be found with this article online at http://dx.doi.org/10.1016/j.celrep.2015.09.046.

AUTHOR CONTRIBUTIONS

Conceptualization, A.D.B., M.C.P.; Methodology, A.D.B, Y.M., R.K., S.Y.K., A.Y.; Software, A.D.B., R.K.; Investigation, A.D.B., Y.M., R.K., T.D.; Resources, Y.Y.; Writing – Original Draft, A.D.B.; Writing – Review & Editing, A.D.B., Y.M., R.K., M.C.P.; Funding Acquisition, A.D.B., M.C.P.

ACKNOWLEDGMENTS

The authors would like to thank Misha Ahrens, Martin Haesemayer, Josua Jordi, and Michael Sidorov for their comments on the manuscript. Li Huei Tsai, Janice Naegele, and Guoping Feng provided transgenic animals. Anusha Narayan, Greg Hale, Sam Cooke, Sebastian Seung, and Kartik Ramamoorthi provided helpful experimental advice. Gerald Schneider was instrumental in interpreting anatomical data. This work was supported by National Eye Institute grant 5R01EY- 014074-18 (M.C.-P.), an NDSEG fellowship (A.D.B.), and an NSF GRFP fellowship (A.D.B.).

Received: May 15, 2015
Revised: August 17, 2015
Accepted: September 15, 2015
Published: October 22, 2015

REFERENCES

Ade, K.K., Wan, Y., Chen, M., Gloss, B., and Calakos, N. (2011). An improved BAC transgenic fluorescent reporter line for sensitive and specific identification of striatonigral medium spiny neurons. Front. Syst. Neurosci. *5*, 32.

Arce, E.A., Bennett-Clarke, C.A., and Rhoades, R.W. (1994). Ultrastructural organization of the noradrenergic innervation of the superficial gray layer of the hamster's superior colliculus. Synapse *18*, 46–54.

Arencibia-Albite, F., Paladini, C., Williams, J.T., and Jiménez-Rivera, C.A. (2007). Noradrenergic modulation of the hyperpolarization-activated cation current (Ih) in dopamine neurons of the ventral tegmental area. Neuroscience *149*, 303–314.

Basso, M.A., and Wurtz, R.H. (1998). Modulation of neuronal activity in superior colliculus by changes in target probability. J. Neurosci. *18*, 7519–7534.

Basso, M.A., and Wurtz, R.H. (2002). Neuronal activity in substantia nigra pars reticulata during target selection. J. Neurosci. *22*, 1883–1894.

Behan, M., Steinhacker, K., Jeffrey-Borger, S., and Meredith, M.A. (2002). Chemoarchitecture of GABAergic neurons in the ferret superior colliculus. J. Comp. Neurol. *452*, 334–359.

Bolton, A.D., Phillips, M.A., and Constantine-Paton, M. (2013). Homocysteine reduces NMDAR desensitization and differentially modulates peak amplitude of NMDAR currents, depending on GluN2 subunit composition. J. Neurophysiol. *110*, 1567–1582.

Busch, A.E., Quester, S., Ulzheimer, J.C., Gorboulev, V., Akhoundova, A., Waldegger, S., Lang, F., and Koepsell, H. (1996). Monoamine neurotransmitter transport mediated by the polyspecific cation transporter rOCT1. FEBS Lett. *395*, 153–156.

Campbell, K.J., Takada, M., and Hattori, T. (1991). Co-localization of tyrosine hydroxylase and glutamate decarboxylase in a subpopulation of single nigrotectal projection neurons. Brain Res. *558*, 239–244.

Cilz, N.I., Kurada, L., Hu, B., and Lei, S. (2014). Dopaminergic modulation of GABAergic transmission in the entorhinal cortex: concerted roles of α1 adrenoreceptors, inward rectifier K^+, and T-type Ca^{2+} channels. Cereb. Cortex *24*, 3195–3208.

Dahlin, A., Xia, L., Kong, W., Hevner, R., and Wang, J. (2007). Expression and immunolocalization of the plasma membrane monoamine transporter in the brain. Neuroscience *146*, 1193–1211.

Dean, P., Redgrave, P., Sahibzada, N., and Tsuji, K. (1986). Head and body movements produced by electrical stimulation of superior colliculus in rats: effects of interruption of crossed tectoreticulospinal pathway. Neuroscience *19*, 367–380.

Dean, P., Redgrave, P., and Westby, G.W. (1989). Event or emergency? Two response systems in the mammalian superior colliculus. Trends Neurosci. *12*, 137–147.

Devoto, P., Flore, G., Saba, P., Fà, M., and Gessa, G.L. (2005a). Stimulation of the locus coeruleus elicits noradrenaline and dopamine release in the medial prefrontal and parietal cortex. J. Neurochem. *92*, 368–374.

Devoto, P., Flore, G., Saba, P., Fà, M., and Gessa, G.L. (2005b). Co-release of noradrenaline and dopamine in the cerebral cortex elicited by single train and repeated train stimulation of the locus coeruleus. BMC Neurosci. *6*, 31.

Dräger, U.C., and Hubel, D.H. (1975). Responses to visual stimulation and relationship between visual, auditory, and somatosensory inputs in mouse superior colliculus. J. Neurophysiol. *38*, 690–713.

Duan, H., and Wang, J. (2010). Selective transport of monoamine neurotransmitters by human plasma membrane monoamine transporter and organic cation transporter 3. J. Pharmacol. Exp. Ther. *335*, 743–753.

Dudkin, E.A., and Gruberg, E.R. (2003). Nucleus isthmi enhances calcium influx into optic nerve fiber terminals in Rana pipiens. Brain Res. *969*, 44–52.

Ewert, J.P. (1984). Tectal mechanisms that underlie prey-catching and avoidance behaviors in toads. In Comparative Neurology of the Optic Tectum, H. Vanegas, ed. (Plenum Press), pp. 247–399.

Felsen, G., and Mainen, Z.F. (2012). Midbrain contributions to sensorimotor decision making. J. Neurophysiol. *108*, 135–147.

Fu, Y., Yuan, Y., Halliday, G., Rusznák, Z., Watson, C., and Paxinos, G. (2012). A cytoarchitectonic and chemoarchitectonic analysis of the dopamine cell groups in the substantia nigra, ventral tegmental area, and retrorubral field in the mouse. Brain Struct. Funct. *217*, 591–612.

Glagow, M., and Ewert, J.P. (1997). Dopaminergic modulation of visual responses in toads. II. Influences of apomorphine on retinal ganglion cells and tectal cells. J. Comp. Physiol. A Neuroethol. Sens. Neural Behav. Physiol. *180*, 11–18.

Glagow, M., and Ewert, J. (1999). Apomorphine alters prey-catching patterns in the common toad: behavioral experiments and (14)C-2-deoxyglucose brain mapping studies. Brain Behav. Evol. *54*, 223–242.

Goddard, C.A., Huguenard, J., and Knudsen, E. (2014). Parallel midbrain microcircuits perform independent temporal transformations. J. Neurosci. *34*, 8130–8138.

Gong, S., Zheng, C., Doughty, M.L., Losos, K., Didkovsky, N., Schambra, U.B., Nowak, N.J., Joyner, A., Leblanc, G., Hatten, M.E., and Heintz, N. (2003). A gene expression atlas of the central nervous system based on bacterial artificial chromosomes. Nature *425*, 917–925.

Gruberg, E., Dudkin, E., Wang, Y., Marín, G., Salas, C., Sentis, E., Letelier, J., Mpodozis, J., Malpeli, J., Cui, H., et al. (2006). Influencing and interpreting visual input: the role of a visual feedback system. J. Neurosci. *26*, 10368–10371.

Gründemann, D., Köster, S., Kiefer, N., Breidert, T., Engelhardt, M., Spitzenberger, F., Obermüller, N., and Schömig, E. (1998). Transport of monoamine transmitters by the organic cation transporter type 2, OCT2. J. Biol. Chem. *273*, 30915–30920.

Haag, C., Berkels, R., Gründemann, D., Lazar, A., Taubert, D., and Schömig, E. (2004). The localisation of the extraneuronal monoamine transporter (EMT) in rat brain. J. Neurochem. *88*, 291–297.

Happel, M.F.K., Deliano, M., Handschuh, J., and Ohl, F.W. (2014). Dopamine-modulated recurrent corticoefferent feedback in primary sensory cortex promotes detection of behaviorally relevant stimuli. J. Neurosci. *34*, 1234–1247.

Helms, M.C., Ozen, G., and Hall, W.C. (2004). Organization of the intermediate gray layer of the superior colliculus. I. Intrinsic vertical connections. J. Neurophysiol. *91*, 1706–1715.

Hemmings, H.C., Jr., Greengard, P., Tung, H.Y., and Cohen, P. (1984). DARPP-32, a dopamine-regulated neuronal phosphoprotein, is a potent inhibitor of protein phosphatase-1. Nature *310*, 503–505.

Hikosaka, O., and Wurtz, R.H. (1985). Modification of saccadic eye movements by GABA-related substances. I. Effect of muscimol and bicuculline in monkey superior colliculus. J. Neurophysiol. *53*, 266–291.

Huerta, M.F., and Harting, J.K. (1984a). The mammalian superior colliculus: studies of its morphology and connections. In Comparative Neurology of the Optic Tectum, H. Vanegas, ed. (Plenum Press), pp. 687–773.

Huerta, M.F., and Harting, J.K. (1984b). Connectional organization of the superior colliculus. Trends Neurosci. *7*, 286–289.

Ikeda, T., and Hikosaka, O. (2003). Reward-dependent gain and bias of visual responses in primate superior colliculus. Neuron *39*, 693–700.

Ikeda, T., and Hikosaka, O. (2007). Positive and negative modulation of motor response in primate superior colliculus by reward expectation. J. Neurophysiol. *98*, 3163–3170.

Illing, R.B. (1996). The mosaic architecture of the superior colliculus. Prog. Brain Res. *112*, 17–34.

Ingle, D. (1975). Focal attention in the frog: behavioral and physiological correlates. Science *188*, 1033–1035.

Isa, T., and Hall, W.C. (2009). Exploring the superior colliculus in vitro. J. Neurophysiol. *102*, 2581–2593.

Jacob, S.N., Ott, T., and Nieder, A. (2013). Dopamine regulates two classes of primate prefrontal neurons that represent sensory signals. J. Neurosci. *33*, 13724–13734.

Johnston, C.A., Cumbay, M.G., Vortherms, T.A., and Watts, V.J. (2001). Adrenergic agonists induce heterologous sensitization of adenylate cyclase in NS20Y-D(2L) cells. FEBS Lett. *497*, 85–89.

Knudsen, E.I. (2011). Control from below: the role of a midbrain network in spatial attention. Eur. J. Neurosci. *33*, 1961–1972.

Krauzlis, R.J., Liston, D., and Carello, C.D. (2004). Target selection and the superior colliculus: goals, choices and hypotheses. Vision Res. *44*, 1445–1451.

Lanau, F., Zenner, M.-T., Civelli, O., and Hartman, D.S. (1997). Epinephrine and norepinephrine act as potent agonists at the recombinant human dopamine D4 receptor. J. Neurochem. *68*, 804–812.

Lovejoy, L.P., and Krauzlis, R.J. (2010). Inactivation of primate superior colliculus impairs covert selection of signals for perceptual judgments. Nat. Neurosci. *13*, 261–266.

Mansour, A., Meador-Woodruff, J.H., Zhou, Q., Civelli, O., Akil, H., and Watson, S.J. (1992). A comparison of D1 receptor binding and mRNA in rat brain using receptor autoradiographic and in situ hybridization techniques. Neuroscience *46*, 959–971.

Mejías-Aponte, C.A., Drouin, C., and Aston-Jones, G. (2009). Adrenergic and noradrenergic innervation of the midbrain ventral tegmental area and retrorubral field: prominent inputs from medullary homeostatic centers. J. Neurosci. *29*, 3613–3626.

Mengod, G., Vilaró, M.T., Niznik, H.B., Sunahara, R.K., Seeman, P., O'Dowd, B.F., and Palacios, J.M. (1991). Visualization of a dopamine D1 receptor mRNA in human and rat brain. Brain Res. Mol. Brain Res. *10*, 185–191.

Merker, B.H. (1980). The sentinel hypothesis: a role for the mammalian superior colliculus. PhD thesis (Massachusetts Institute of Technology).

Metzger, M., Britto, L.R.G., and Toledo, C.A.B. (2006). Monoaminergic markers in the optic tectum of the domestic chick. Neuroscience *141*, 1747–1760.

Mize, R.R., Luo, Q., Butler, G., Jeon, C.J., and Nabors, B. (1992). The calcium binding proteins parvalbumin and calbindin-D 28K form complementary patterns in the cat superior colliculus. J. Comp. Neurol. *320*, 243–256.

Mooney, R.D., Bennett-Clarke, C., Chiaia, N.L., Sahibzada, N., and Rhoades, R.W. (1990). Organization and actions of the noradrenergic input to the hamster's superior colliculus. J. Comp. Neurol. *292*, 214–230.

Müller, J.R., Philiastides, M.G., and Newsome, W.T. (2005). Microstimulation of the superior colliculus focuses attention without moving the eyes. Proc. Natl. Acad. Sci. USA *102*, 524–529.

Northmore, D.P., Levine, E.S., and Schneider, G.E. (1988). Behavior evoked by electrical stimulation of the hamster superior colliculus. Exp. Brain Res. *73*, 595–605.

Odagaki, Y., Dasgupta, S., and Fuxe, K. (1995). Additivity and non-additivity between dopamine-, norepinephrine-, carbachol- and GABA-stimulated GTPase activity. Eur. J. Pharmacol. *291*, 245–253.

Onali, P., Olianas, M.C., and Gessa, G.L. (1985). Characterization of dopamine receptors mediating inhibition of adenylate cyclase activity in rat striatum. Mol. Pharmacol. *28*, 138–145.

Phillips, M.A., Colonnese, M.T., Goldberg, J., Lewis, L.D., Brown, E.N., and Constantine-Paton, M. (2011). A synaptic strategy for consolidation of convergent visuotopic maps. Neuron *71*, 710–724.

Phongphanphanee, P., Mizuno, F., Lee, P.H., Yanagawa, Y., Isa, T., and Hall, W.C. (2011). A circuit model for saccadic suppression in the superior colliculus. J. Neurosci. *31*, 1949–1954.

Robinson, D.A. (1972). Eye movements evoked by collicular stimulation in the alert monkey. Vision Res. *12*, 1795–1808.

Schärer, Y.P.Z., Shum, J., Moressis, A., and Friedrich, R.W. (2012). Dopaminergic modulation of synaptic transmission and neuronal activity patterns in the zebrafish homolog of olfactory cortex. Front. Neural Circuits *6*, 76.

Schiller, P.H., and Stryker, M. (1972). Single-unit recording and stimulation in superior colliculus of the alert rhesus monkey. J. Neurophysiol. *35*, 915–924.

Schott, B.H., Frischknecht, R., Debska-Vielhaber, G., John, N., Behnisch, G., Düzel, E., Gundelfinger, E.D., and Seidenbecher, C.I. (2010). Membrane-Bound Catechol-O-Methyl Transferase in Cortical Neurons and Glial Cells is Intracellularly Oriented. Front. Psychiatry *1*, 142.

Schultz, W. (2007). Multiple dopamine functions at different time courses. Annu. Rev. Neurosci. *30*, 259–288.

Sotnikova, T.D., Beaulieu, J.-M., Espinoza, S., Masri, B., Zhang, X., Salahpour, A., Barak, L.S., Caron, M.G., and Gainetdinov, R.R. (2010). The dopamine metabolite 3-methoxytyramine is a neuromodulator. PLoS ONE *5*, e13452–e13459.

Sperry, R.W. (1963). Chemoaffinity in the orderly growth of nerve fiber patterns and connections. Proc. Natl. Acad. Sci. USA *50*, 703–710.

Tecuapetla, F., Patel, J.C., Xenias, H., English, D., Tadros, I., Shah, F., Berlin, J., Deisseroth, K., Rice, M.E., Tepper, J.M., and Koos, T. (2010). Glutamatergic signaling by mesolimbic dopamine neurons in the nucleus accumbens. J. Neurosci. *30*, 7105–7110.

Thibault, D., Loustalot, F., Fortin, G.M., Bourque, M.J., and Trudeau, L.E. (2013). Evaluation of D1 and D2 dopamine receptor segregation in the developing striatum using BAC transgenic mice. PLoS ONE *8*, e67219.

Trapnell, C., Williams, B.A., Pertea, G., Mortazavi, A., Kwan, G., van Baren, M.J., Salzberg, S.L., Wold, B.J., and Pachter, L. (2010). Transcript assembly and quantification by RNA-seq reveals unannotated transcripts and isoform switching during cell differentiation. Nat. Biotechnol. *28*, 511–515.

Tritsch, N.X., Ding, J.B., and Sabatini, B.L. (2012). Dopaminergic neurons inhibit striatal output through non-canonical release of GABA. Nature *490*, 262–266.

Tunbridge, E.M., Harrison, P.J., Warden, D.R., Johnston, C., Refsum, H., and Smith, A.D. (2008). Polymorphisms in the catechol-O-methyltransferase (COMT) gene influence plasma total homocysteine levels. Am. J. Med. Genet. B. Neuropsychiatr. Genet. *147B*, 996–999.

Versteeg, D.H., Van Der Gugten, J., De Jong, W., and Palkovits, M. (1976). Regional concentrations of noradrenaline and dopamine in rat brain. Brain Res. *113*, 563–574.

Vokoun, C.R., Jackson, M.B., and Basso, M.A. (2010). Intralaminar and interlaminar activity within the rodent superior colliculus visualized with voltage imaging. J. Neurosci. *30*, 10667–10682.

Wang, Y., Kakizaki, T., Sakagami, H., Saito, K., Ebihara, S., Kato, M., Hirabayashi, M., Saito, Y., Furuya, N., and Yanagawa, Y. (2009). Fluorescent labeling of both GABAergic and glycinergic neurons in vesicular GABA transporter (VGAT)-venus transgenic mouse. Neuroscience *164*, 1031–1043.

Weller, M.E., Rose, S., Jenner, P., and Marsden, C.D. (1987). In vitro characterisation of dopamine receptors in the superior colliculus of the rat. Neuropharmacology *26*, 347–354.

Wurtz, R.H., and Mohler, C.W. (1976). Organization of monkey superior colliculus: enhanced visual response of superficial layer cells. J. Neurophysiol. *39*, 745–765.